

Experimental study on the oscillation of a separating shear layer in a cavity

Y. Inoue & S. Yamashita

*Department of Mechanical and Systems Engineering,
Gifu University, Japan*

Abstract

This study was performed to clarify the oscillation of a separating shear layer in a cavity formed peripherally on a cylinder in a uniform axial stream. Experiments were conducted on the cavity having the width-depth ratio of 4 and formed in a water channel. Firstly, the dynamic characteristics of the flow field were investigated by visualizing the flow, and a time-averaged flow field was measured with a particle imaging velocimetry (PIV). As a result, the typical three flow patterns were demonstrated. Secondly, spatiotemporal measurements were taken along and/or across the shear layer with a UVP monitor. Thirdly, the proper orthogonal decomposition was applied to the UVP dataset, and random coefficients at the low-order POD modes were examined. As a result, two dominant time scales of $f b/U_m = 0.1$ and 0.9 were found in the shear layer. These two-scale flow structures can be shown through filtration with discrete wavelet transformation.

Keywords: cavity flow, self-sustaining oscillation, ultrasonic Doppler method, wavelet analysis, POD.

1 Introduction

In many cases, the flow passing across an open cavity generates self-excited oscillation, causing two major problems: radiating noise and fluid induced oscillation. Although the characteristics of cavity oscillation have been studied in recent decades, there are still some problems that remain unsolved even today. The details of these problems were perused by Rockwell and Naudascher [1] and Grace [2] in their prospective papers and by Lin and Rockwell [3] and Howe [4].



Rockwell and Naudascher [1] describe the self-excited oscillation by dividing it into three types, where the cavity oscillation under this study falls into a type caused by flow-specific instability according to their classification. Lin and Rockwell [3] describe the characteristics of the cavity oscillation in four steps: (i) interaction between a vorticity concentrated area and a downstream cavity edge, (ii) effects on a shear layer formed from an upstream edge, (iii) conversion to fluctuations in a separating shear layer, and (iv) amplification in the flow direction of this conversion. They comment that the sequence of these four steps is not stable in terms of time, and the instantaneous velocities in the direction along the shear layer should be measured. On the other hand, Grace [2] investigates the math calculation for cavity noise prediction, and Howe [4] treats the same subject theoretically.

This study is intended to experimentally clarify the flow field of an axisymmetric cavity on a cylinder placed in an axial flow. In this paper, a cylinder with a water channel of the aspect ratio of four is set up in a uniform water flow, instantaneous fluctuation velocities are measured with an ultrasonic velocity profiler (UVP monitor) [5], and the characteristics of the oscillation of the separating shear layer are studied from the results of the measurement.

The axisymmetric cavity was studied in detail by Sarohia [6], and the effects of the boundary layer thickness of the approaching flow, Reynolds number and the aspect ratio of the cavity on self-excited oscillation characteristics were clarified. Later, Gharib [7] studied the effects of periodic disturbance introduced into the approach flow, and Gharib and Roshko [8] studied the relationship between the drag acting on the cavity and the flow pattern. On the other hand, as to the instantaneous flow field, Rockwell and Knisely [9, 10] and Neary and Stephanoff [11] showed their experiments in the visualization of flow, and Lin and Rockwell [3] and Meganathan and Vakili [12] showed their experiments with a particle imaging velocimetry (PIV).

In this study, the basic flow patterns were studied through visualized flow observation by using the dye streak method, and then the mean velocity field was shown based on the results of measurement with the PIV. The spatiotemporal velocity information was measured with the UVP, and the low-order model of the separating shear layer in self-excited oscillation was identified through the mode analysis of the acquired data. The UVP method is detailed by Takeda [5].

2 Experimental apparatus and procedures

The experiment of this study was conducted by using a low-speed recirculating water channel. The measurement part of this channel was 0.7 m wide and 2.2 m long. The test body was an acrylic resin cylinder with the radius $a = 100$ mm having a streamlined head of aluminium alloy casting. The downstream end of the cylinder was fixed to a frame, which was independent of the tank. The posture of the cylinder toward the flow was adjusted with three wires located in the upstream part. The outline of the flow field and its coordinate system are shown in fig. 1. The main stream direction is taken to be the x -axis, the radial direction to be the z -axis and circumferential direction to be the y -axis. The

cavity was shaped with the width $b = 100$ mm and the depth $h = 25$ mm. Assuming that the reference velocity of the main stream outside the layer was expressed as U_m , the experiment was conducted as to the reference Reynolds number $Re = 0.6 \times 10^4$ and 1.0×10^4 , where $Re = U_m b / \nu$. At this time, the boundary layer of the approach flow was laminar, and the momentum thickness was $\theta_0 = 1.38$ mm ($b/\theta_0 = 71$) at $Re = 1.0 \times 10^4$ and $x = -10$ mm.

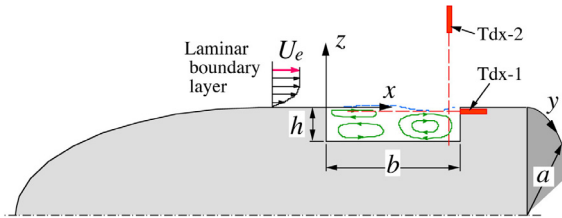


Figure 1: Flow field and coordinate system.

The flow visualization was realized by injecting fluorescence dye Rhodamine B from three small openings ($\phi 1$ mm) at $x = -20$ mm upstream from the cavity and $x = 20$ mm and 80 mm within the cavity, and illuminated by an Nd:Yag laser sheet light source. In the PIV method, Ar-ion laser was used for illumination, and a $1k \times 1k$ pixel digital camera SKC-100 and Digital Frame Grabber IPM-8540D were used for imaging at 15 frames/sec. Polymer spheres having the mean size of $180 \mu\text{m}$ were used as tracer particles, and the cross-correlation method was used for velocity analysis.

The data measured with the UVP is realized as the spatiotemporal distribution of instantaneous velocity components in the ultrasonic beam flying direction. In this experiment, as shown in fig. 1, ultrasonic transducers (frequency: 8MHz, beam diameter: 2.5 mm) were positioned axially (Tdx-1) and radially (Tdx-2), and $\tilde{u}(x, t)$ and $\tilde{w}(z, t)$ were measured respectively. The transducer Tdx-1 was embedded in the cylinder, and its center position was $z = -7$ mm. The transducer Tdx-2 was attached to the tip-end of the supporting rod having a wing cross-sectional profile, and moved axially within the range of $x = 30$ to 90 mm by using a traverser. For ultrasonic scattering particles, hydrogen bubbles generated from a Pt wire having the diameter of $30 \mu\text{m}$ were used. The velocity distribution sampling intervals of Tdx-1 and Tdx-2 were 32 ms and 50 ms, respectively, when these transducers were used independently. When a multiplexer was used and Tdx-1 and Tdx-2 were used concurrently and alternately while they were switched to each other, the switching time interval was 40 ms. As to the UVP data, the proper orthogonal decomposition (POD) method [13] was applied to the extraction of the spatial mode, and the Fourier transformation and the discrete wavelet transformation were applied to the analysis of the time fluctuation components. The details of this data processing are left out here (refer to [13]).

3 Experimental results and considerations

3.1 Visualization of flows

Figure 2 shows the visualized images of flows within the cavity, arranged for each of three typical flow patterns in four frames each as the time passes (from top to bottom). The main stream flows from left to right. In any flow pattern, the streakline from the upstream cavity edge to the downstream is broken almost in the middle of the cavity width, causing a large deformation in the downstream. The appearance of this deformation differs among the three patterns as shown. The tip of the streak collides with the downstream cavity edge in fig. 2(a), the streak tip is caught up in the cavity without break in fig. 2(b), and the streakline collides little with the downstream edge and flows off as it is downward in fig. 2(c). When it comes to the flow within the cavity, it is active in a comparatively compact area near the downstream in fig. 2(a), a large-scaled flow pattern occupying more than half of the cavity area is formed in fig. 2(b), and the degree of activity of flow is lower compared with the former and there is little flow recirculation within the cavity in fig. 2(c).

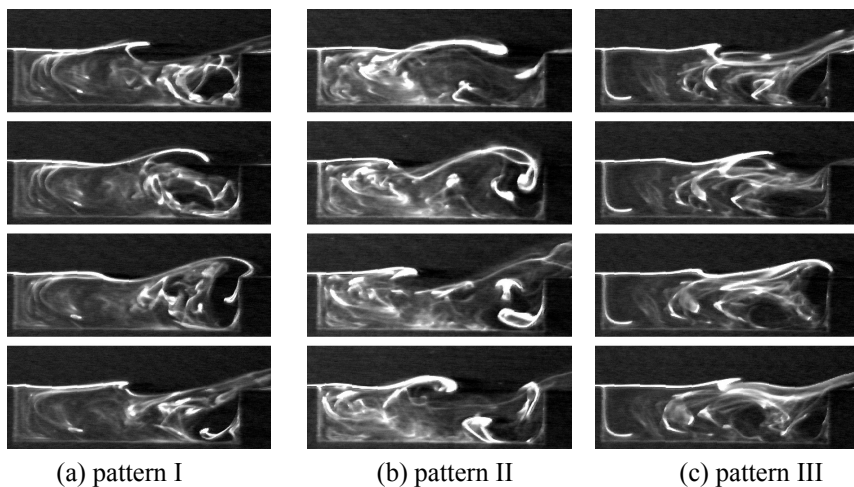


Figure 2: Typical flow patterns visualized by dye injection.

These integrated streaklines in fact represent certain realized flow patterns of all flow patterns existent numerously. As a result of observation, these three flow patterns were confirmed to be typical ones. As Lin and Rockwell [3] point out, the cause of the pattern fluctuation has not yet been identified clearly. While responsive jitters and relativity of three-dimensionality are thought of as possible causes, there have been few studies treating this subject actively (e.g. [10] and [11]).

3.2 Mean flow field

Figure 3 shows the mean behaviour in the x - z plane measured by the PIV method as $Re = 0.6 \times 10^4$. In fig. 3(a) showing the mean velocity vectors, a definite main vortex can be seen in an area occupying about half on the downstream side of the cavity width. The main vortex reaches the cavity bottom, and a boundary layer develops above the bottom. This boundary layer separates from the bottom and flows upward. Upon reaching the separating shear layer of the main stream, it forms a saddle point. In contrast with this, the flow on the upstream side of the saddle point is extremely weak, and the secondary vortex driven by the entrainment of the shear layer and another secondary vortex in reverse rotation to the main vortex are formed as shown schematically in fig. 3(b). Each letter in the figure indicates a singular point. N stands for node, S stands for saddle, N' stands for half-node and S' stands for half-saddle.

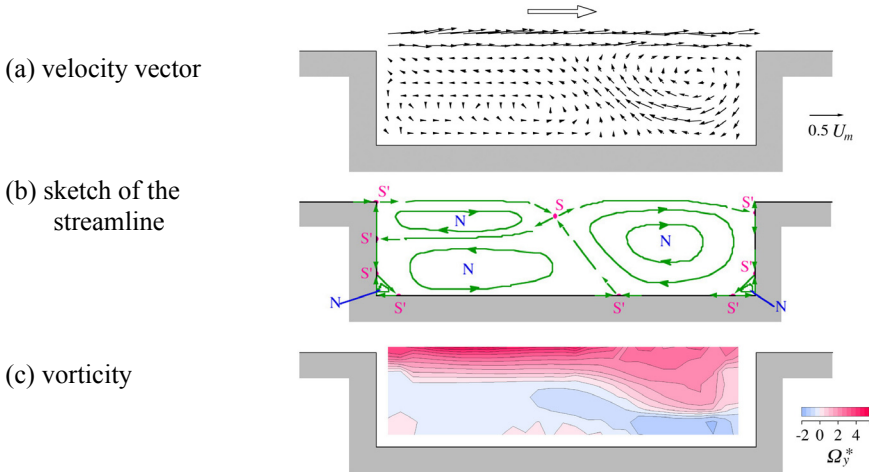


Figure 3: Time-averaged spatial maps measured with the PIV at $Re = 0.6 \times 10^4$.

Figure 3(c) shows the contour lines of the dimensionless vorticity component in the y -direction, Ω_y^* , defined as the following;

$$\Omega_y^* = \frac{\Omega_y}{U_m/b} = \frac{b}{U_m} \left(\frac{\partial U}{\partial z} - \frac{\partial W}{\partial x} \right). \quad (1)$$

It was calculated by numerical differentiation from the mean velocity field by using the least-square method of quintic polynomial. In the separating shear layer, there is an area showing positive vorticity corresponding to $\partial U/\partial z > 0$. The width of this area expands drastically at $x/b > 0.5$, filling most areas of the main vortex but without excessive concentration. The bottom boundary layer shows $\partial U/\partial z < 0$, generating negative vorticity. This area showing the negative vorticity is transferred into the cavity upon the separation of the bottom boundary layer.

3.3 Fluctuation energy

In this study, paying attention to the oscillation pattern of the shear layer, measurement was taken by the UVP method in the direction along the shear layer longitudinally (Tdx-1) and in the direction across the shear layer (Tdx-2), and the oscillation mode was analyzed. Figure 4 shows axial changes in the fluctuation velocity energy as u^2 quantified by Tdx-1, E_w quantified by Tdx-2 and w^2 at $z = 0$. Here, E_w expresses the total fluctuation energy within the measurement range defined by

$$E_w = \frac{1}{T} \iint w^2(z, t) dt dz = \sum_n \lambda_w^{(n)}, \quad (2)$$

and \bar{E}_w is the spatial mean value of E_w . The distribution of u^2 increases gradually up to $x/b < 0.6$, and then increases rapidly toward the peak of $x/b \approx 0.85$. The distribution of the radial components shows almost the same trend, but the fluctuation energy at $x/b < 0.4$ is considerably smaller. $\lambda_w^{(n)}$ in eqn. (2) expresses the eigenvalue that can be obtained empirically by using the POD method [13]. When the eigenfunction corresponding to each mode is expressed as $\phi_w^{(n)}$, the original velocity data can be expressed by

$$w(z, t) = \sum_n w^{(n)}(t) \phi_w^{(n)}(z). \quad (3)$$

Here, $w^{(n)}$ is the n th random coefficient. Since the norm of $\phi_w^{(n)}$ itself is normalized to 1, the square mean value of the random coefficient is equal to the eigenvalue $\lambda_w^{(n)}$. That is, even though there is an issue of the distribution profile of the eigenfunction, the spatiotemporal information of the UVP data can be contracted to the time change in the random coefficient.

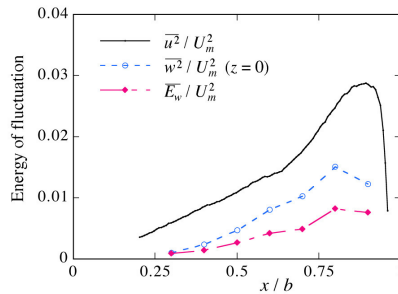


Figure 4: Axial change in the energy of velocity fluctuation.

The POD was applied to the data within the range of $x/b = 0.5$ to 1, and the estimated POD spectra are shown as to $Re = 0.6 \times 10^4$ and 1.0×10^4 in fig. 5(a). The spectra were normalized by the total fluctuation energy E_u . In both cases of Re , the spectra shown are almost the same. Only the first mode captures about 50% of the total fluctuation energy, and the first three modes contain over 80% of the total fluctuation energy. Here, due to limitations of space, the distribution

of the eigenfunction has to be omitted, but it should be noted here that the eigenfunction takes the sine-wave distribution with different wavelengths and phases depending on the mode. Also in the radial direction (fig. 5(b)), most fluctuation energy is captured in the lower-order modes, and the energy content rate of the first mode is slightly high at $x/b = 0.8$. The eigenfunction is expressed by the even and odd function taking the center of the shear layer as an axis of symmetry, whose distribution profile has no essential difference due to the axial position.

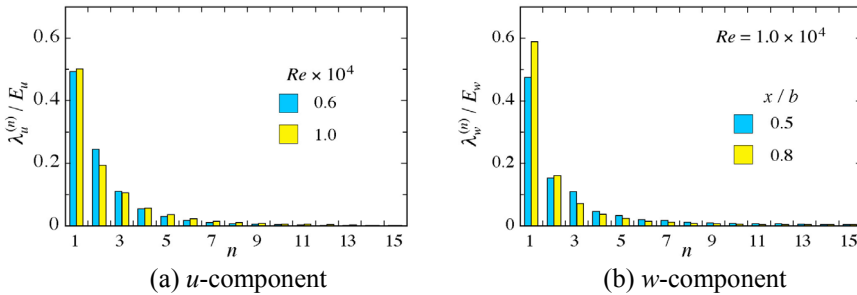


Figure 5: POD spectra of velocity fluctuation.

The power spectra of the axial and radial random coefficients were normalized by U_m^2 as to $n = 1$ to 5 as shown in fig. 6. From these figures, it is understood that there are two typical time scales in the present flow and they coexist with a comparatively sharp peak of the dimensionless frequency of about 0.9 and the peak of the broad bandwidth centered about the dimensionless frequency of 0.1. The former peak corresponds to the self-excited oscillation and has its dominance in each spectrum excepting the axial spectrum of $Re = 1.0 \times 10^4$. In the radial direction, the spectral peak is sharper at $x/b = 0.5$. On the other hand, the long-period fluctuation of the dimensionless frequency of 0.1 is made apparent well in the spectra of $u^{(1)}$.

3.4 Oscillation pattern of shear layer

Here, to separate these two time scales and examine their oscillating modes, the random coefficient of the axial velocity distribution was subjected to discrete wavelet transformation. Daubechies with $N = 4$ was used for the mother wavelet. The wavelet spectrum was normalized by U_m^2 as shown in fig. 7. In the abscissa scale j , when $j = 0$ is the sampled signal level, the resolution degrades sequentially as $j = -1, -2, \dots$ down to the lowest frequency at $j = -10$. As understood from this figure, the random coefficients of the POD mode $n = 1$ show their peaks at $j = -5$ and -8 , while the random coefficients of the POD mode $n = 2$ and 3 show their peaks only at $j = -5$. Here, the dimensionless Nyquist frequency at $j = -5$ is about 0.8.

The random coefficients were inverse transformed by using $j = -5$ to -10 ($\bar{u}_{-4}^{(n)}$), $j = -5$ to -6 ($\tilde{u}_{-5}^{(n)} + \tilde{u}_{-6}^{(n)}$) and $j = -7$ to -10 ($\bar{u}_{-6}^{(n)}$) of all wavelet coefficients of each scale, and then the velocity field was reconstructed by using

the eigenfunction as shown in fig. 8. It is understood from this figure that the long and short scale flow structures are separated well (figs. 8(b) and 8(c)). That is, the long-period fluctuation can be captured by $\bar{u}_{-6}^{(1)}$, having the contribution of over 25% of the total fluctuation energy.

Lastly, correlation between the axial fluctuation and the radial fluctuation was studied. Figure 9 shows the random coefficients of the first mode and second mode as to the axial data and the radial data ($x/b = 0.8$). There is the lag of the dimensionless time of 0.04 between these two directional components due to a measurement problem. The positive and negative signs of the random coefficient are dependent on the eigenfunction. The time delay τ was varied and the correlation coefficient between the random coefficients was obtained as shown in fig. 10. The correlation between $u^{(1)}$ vs. ($w^{(1)}$ or $w^{(2)}$) is identical to the distribution of the time scale corresponding to the long-period fluctuation, where radial inflow and outflow repeats along with the repetition of the slow acceleration and deceleration of the axial velocity. Between $u^{(2)}$ vs. ($w^{(1)}$ or $w^{(2)}$), the correlation distribution is seen in response to the self-excited oscillation period but their correlation is weak.

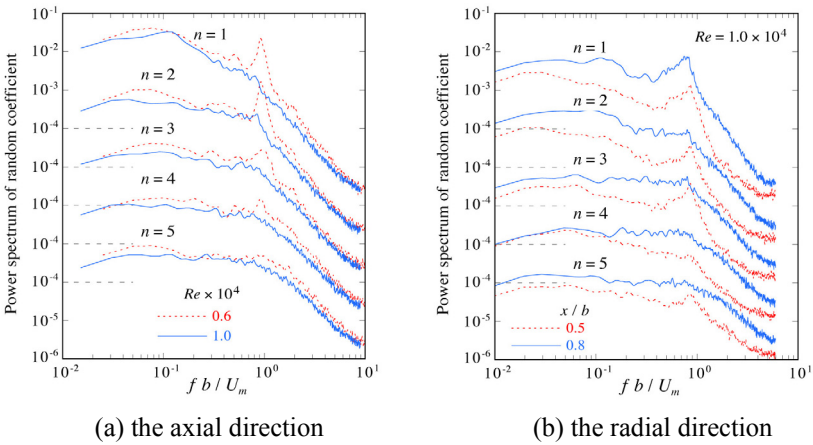


Figure 6: Power spectra of the random coefficient.

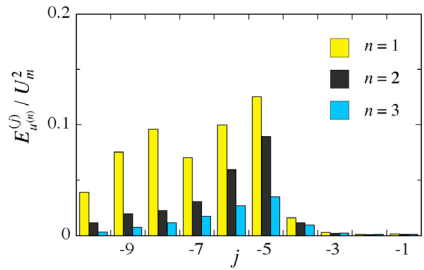


Figure 7: Wavelet spectrum of the random coefficient in the axial direction at $Re = 0.6 \times 10^4$.



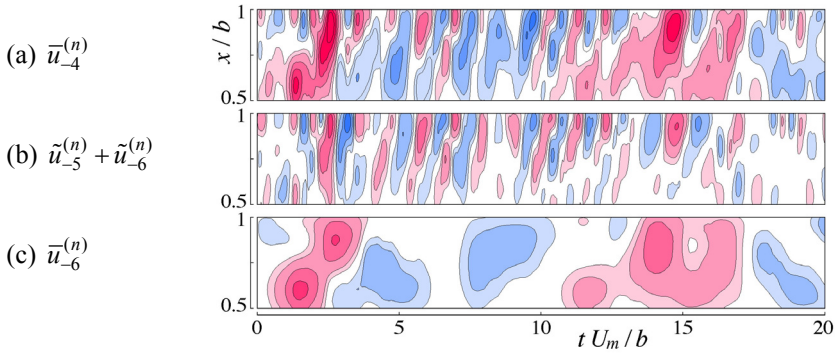


Figure 8: Velocity maps reconstructed with the first three modes.

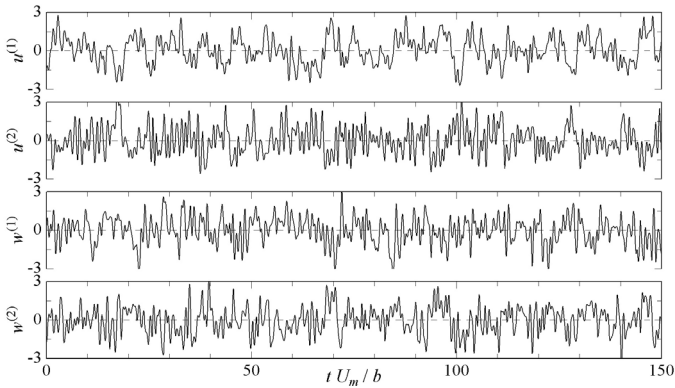


Figure 9: Traces of the random coefficients at the first two POD-modes for $u(x, t)$ and $w(z, t)$ at $x/b = 0.8$, which were simultaneously measured.

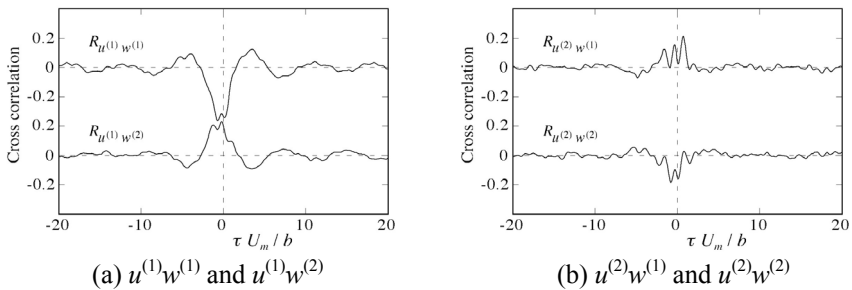


Figure 10: Correlation between the random coefficients at the two POD modes.

4 Conclusions

The results of this study are summarized as follows:

- (1) Three patterns of flow fields were demonstrated according to the mode of interaction between the separating shear layer and the downstream cavity edge through visualized observation. Also, the mean velocity and vorticity within the water channel were defined through velocity measurement by the PIV, and streakline patterns were shown schematically.
- (2) Axial and radial measurements were taken by the UVP, and the measurement results were analyzed by the POD. In both directions, fluctuation energy over 80% was captured in three low-order modes. From the power spectra of the random coefficients, the dominances of two time scales were demonstrated.
- (3) When the time scales of the random coefficient were separated by using the discrete wavelet transformation and then reconstructed, the flow structures of the two scales could be separated and examined.

References

- [1] Rockwell, D. & Naudascher, E., Review - self-sustaining oscillations of flow past cavities. *Trans. ASME: J. Fluids Eng.*, **100**, pp. 152-165, 1978.
- [2] Grace, S.M., An overview of computational aeroacoustic techniques applied to cavity noise prediction. *AIAA Paper* 2001-0510, 2001.
- [3] Lin, J.-C. & Rockwell, D., Organized oscillations of initially turbulent flow past a cavity. *AIAA J.*, **39**, pp. 1139-1151, 2001.
- [4] Howe, M. S., Edge, cavity and aperture tones at very low mach numbers. *J. Fluid Mech.*, **330**, pp. 61-84, 1997.
- [5] Takeda, Y., Velocity profile measurement by ultrasonic Doppler method. *Exp. Thermal & Fluid Sci.*, **10**, pp. 444-453, 1995.
- [6] Sarohia, V., Experimental investigation of oscillations in flows over shallow cavities. *AIAA J.*, **15**, pp. 984-991, 1977.
- [7] Gharib, M., Response of the cavity shear layer oscillations to external forcing. *AIAA J.*, **25**, pp. 43-47, 1987.
- [8] Gharib, M. & Roshko, A., The effect of flow oscillations on cavity drag. *J. Fluid Mech.*, **177**, pp. 501-530, 1987.
- [9] Rockwell, D. & Knisely, C., The organized nature of flow impingement upon a corner. *J. Fluid Mech.*, **93**, pp. 413-432, 1979.
- [10] Rockwell, D. & Knisely, C., Observations of the three-dimensional nature of unstable flow past a cavity. *Phys. Fluids*, **23**, pp. 425-431, 1980.
- [11] Neary, M.D. & Stephanoff, K.D., Shear-layer-driven transition in a rectangular cavity. *Phys. Fluids*, **30**, pp. 2936-2946, 1987.
- [12] Meganathan, A.J. & Vakili, A.D., An experimental study of open cavity flows at low subsonic speeds. *AIAA Paper* 2002-0280, 2002.
- [13] Inoue, Y., Yamashita, S. & Kondo, K., The ultrasonic velocity profile measurement of flow structure in the near field of a square free jet. *Exp. Fluids*, **32**, pp. 170-178, 2002.

